ACS APPLIED MATERIALS & INTERFACES

www.acsami.org

Research Article

Close-Packed Ultrasmooth Self-assembled Monolayer of $CsPbBr_3$ Perovskite Nanocubes

Biplab K. Patra,[⊥] Harshal Agrawal,[⊥] Jian-Yao Zheng, Xun Zha, Alex Travesset, and Erik C. Garnett*

Cite This: *ACS Appl. Mater. Interfaces* 2020, 12, 31764–31769

Read Online

ACCESS | Metrics & More | Article Recommendations | Supporting Information

ABSTRACT: The use of colloidal self-assembly to form the complex multiscale patterns in many optoelectronic devices has been a long-standing dream of the nanoscience community. While great progress has been made using charged colloids in polar solvents, controlled assembly from nonpolar solvents is much more challenging. The major challenge is colloidal clustering caused by strong van der Waals (vdW) attraction between long-chain surface capping ligands passivating the surface of nanocrystals. Such clustering degrades ordering in packing during the self-assembly process. While ligand exchange to provide colloidal stability in polar phases is often an option, this is not the case for the exciting new class of halide perovskites due to the material's solubility in essentially all polar solvents. Here, we report surface-functionalized self-assembly of luminescent $CsPbBr_3$ perovskite nanocubes by partially replacing long-chain oleyl groups (18 carbon chain) with short-chain thiocyanate (SCN^-). This enables the fabrication of ultrasmooth monolayer thin films of nanocubes with a root-mean-square (RMS) roughness of around 4 Å. This ultrasmooth large area self-assembled layer could act as high-efficiency optoelectronic devices like solar cells, light-emitting diodes (LEDs), transistors, etc. We correlate our experimental results with simulations, providing detailed predictions for lattice constants with chain conformations showing reduced free energy for cubes grafted with short-chain thiocyanate compared to long-chain oleyl groups, thus facilitating better self-assembly.

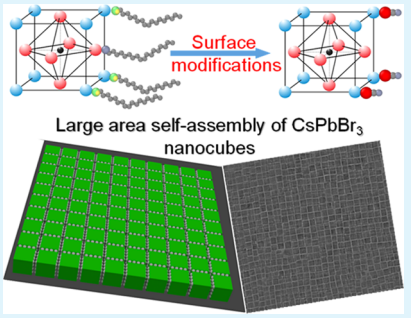

KEYWORDS: *halide perovskites, nanocubes, ligand exchange, surface modification, monolayer self-assembly*

INTRODUCTION

Self-assembly of nanomaterials to form complex two-dimensional (2D) and three-dimensional (3D) patterns with control from nanometer to centimeter length scale has been a long-standing challenge for the nanoscience community.[1−7] The prospect of engineering complex functional devices by simple wet chemistry and self-assembly has largely been inspired by nature, where hierarchical ordering and reproducible complex pattern formation are achieved at or near room temperature in an aqueous environment.[8,9] Although there has been tremendous progress in bioinspired and colloidal self-assembly, most work has been conducted either in polar solvents with charged colloids[3] or at the interface between polar and nonpolar solvents.[10] In polar solvents, surface charges on nanoparticles provide excellent colloidal stability ensuring facile monolayer 2D[11,12] and 3D[3] self-assembly and patterning via capillary assembly[13] or electrophoretic deposition.[14] In nonpolar solvents, they can be stabilized using soluble organic surface capping ligands[15] and self-assembly proceeds, for example, via solvent evaporation[4,16−21] and nanoimprinting.[22] However, the colloidal aggregation due to strong van der Waals (vdW) interactions[23,24] between organic chains prevents controlled assembly into single-crystalline monolayers. The role of capping ligands therefore is not only to ensure stability but also to guide self-assembly into ordered or disordered structures.

There is an emerging class of materials, namely the halide perovskite nanocrystals,[25−27] which has outstanding optoelectronic properties. The most stable inorganic perovskite $CsPbBr_3$ nanostructures[25,28−32] are stabilized by long-chain oleyl groups as surface capping ligands. Nanocubes of $CsPbBr_3$ have a tendency to fuse into single crystals,[33−36] making them ideally suited for a self-assembled thin film and luminescent nanopatterned devices. However, the major problem behind their self-assembly is that due to their ionic nature they readily dissolve in a polar environment, while in a nonpolar solvent, they have a tendency to cluster[37] due to strong vdW attractions between the long capping ligands. Therefore, preventing colloidal aggregation to enable close-packed monolayer thin films remains an open challenge. Here, we demonstrate that besides improving the optical quality,[38] short-chain thiocyanate ligands also lead to a substantial reduction in cube−cube

Received: March 31, 2020
Accepted: June 17, 2020
Published: June 17, 2020

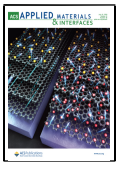

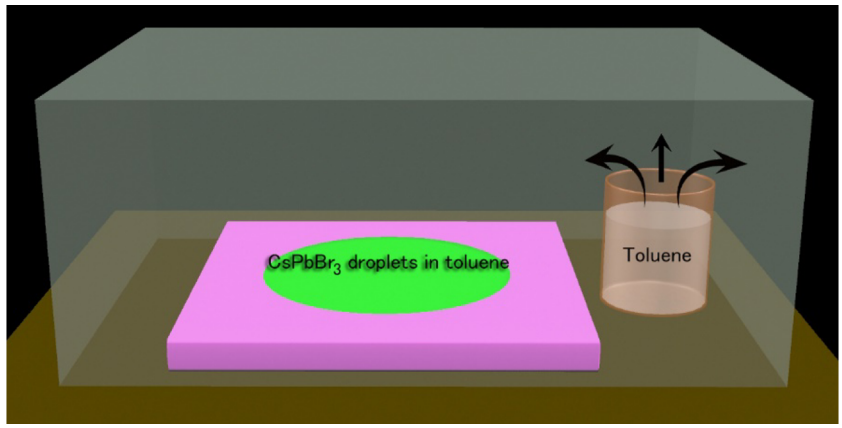

Figure 1. Schematic presentation of droplet evaporation technique inside a closed chamber to get a close-packed monolayer self-assembly.

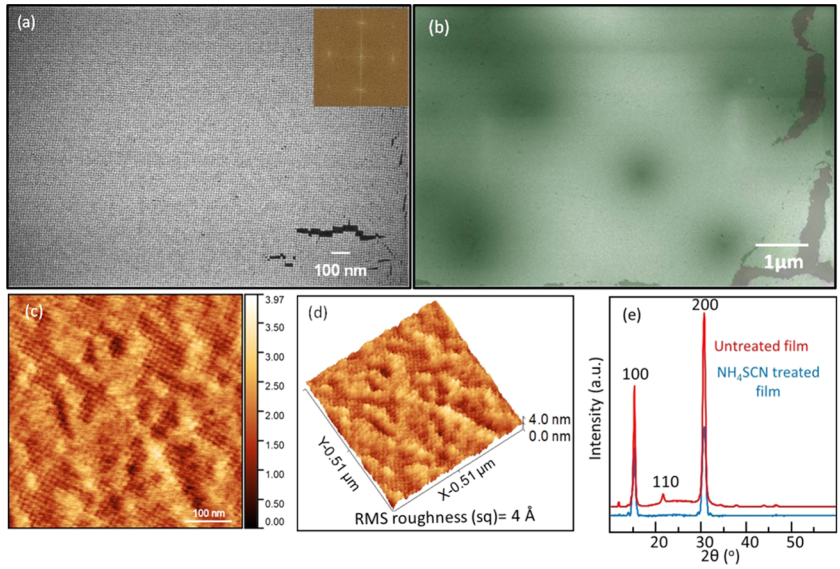

Figure 2. (a) High-resolution scanning electron microscopy (SEM) image of the monolayer; inset of (a) shows FFT pattern of the monolayer film. (b) Low-resolution SEM image of a self-assembled $CsPbBr_3$ nanocube monolayer. Light green false color is used in the SEM image to indicate the nanocube monolayer on Si (black area). (c) Atomic force microscopy (AFM) image of a monolayer film. (d) Three-dimensional view of the area in (c) and measured RMS roughness value. (e) X-ray diffraction (XRD) pattern of monolayer (NH_4SCN-treated film) and multilayer (untreated with NH_4SCN) nanocube assembly.

interactions, greatly improving self-assembly. This enables the formation of monolayer thin films with root-mean-square (RMS) roughness of 4 Å.

RESULTS AND DISCUSSION

We perform colloidal synthesis of monodispersed $CsPbBr_3$ nanocubes using a modified literature report,[28] and carry out surface modifications to achieve better control in self-assembly (details in the Experimental Section). In short, lead bromide ($PbBr_2$), octadecene (ODE), oleic acid (OAc), and oleylamine (OAm) are heated at 200 °C in a three-necked round bottom flask. Cesium oleate is injected, and 5 s after the injection, the temperature is decreased to 160 °C.

The reaction mixture is then annealed at 160 °C for 10 min. Annealing at this stage is essential to obtain monodispersed cubes with sharp facets, which is crucial for a long-range, defect-free, close-packed ordering of cubes. After that, long-chain oleyl groups on the nanocube surfaces are partially exchanged with shorter-chain thiocyanate (details in the Experimental Section). The thiocyanate-capped cubes dispersed in toluene are dropcast on a silicon (Si) substrate, with slow evaporation of toluene (Figure 1), leading to a beautiful monolayer assembly of cubes with uniform packing, as shown in Figure 2a.

A low-resolution SEM image of the film is shown in Figure 2b (also in Figure S1), showing large area continuous assembly on a Si substrate. The assembled layer is truly a monolayer, shown in Figure S2, observed from the fact that the cleaning procedure (rinse one time with methyl acetate solution very gently) used to avoid charging effects during SEM led to partial delamination in a few places. The AFM image in Figure 2c,d reveals that the surface of the assembled monolayer is ultrasmooth, with a measured RMS roughness of 4 Å (Figure 2d). The surface of the nanocubes is atomically flat; the 4 Å roughness can be attributed to residual ligands crystallized on the surface after solvent evaporation and size dispersion of the nanocubes. RMS value of an entirely different part of the assembly shows similar roughness (Figure S3), indicating the uniform nature of surface roughness throughout the whole sample. Assemblies of the as-synthesized (without thiocyanate

https://dx.doi.org/10.1021/acsami.0c05945
ACS Appl. Mater. Interfaces 2020, 12, 31764−31769

exchange) cubes result in short-ranged domains, mostly with multilayer stacking, as shown in Figure S4. Quantitative measurement of the height profile from AFM of different layers stacking is shown in Figure S5. We have analyzed the crystallographic orientation of close-packed monolayer films and multilayer stacked films using XRD, presented in Figure 2e. In both cases, the peak corresponding to the [100] direction is the strongest, but thiocyanate-capped nanocube films only have [100] and their equivalent peak contributions, which can be attributed to the fact that these cubes are aligned along the same [100] crystallographic orientations to form a close-packed film. This is also clear from the SEM images where even before ligand exchange (Figure S4) there is reasonably good ordering, though often multilayers rather than monolayers prevent perfect ordering. This imperfect ordering leads to the substantial 110 reflection shown in the untreated sample (Figure 2e), which is absent after thiocyanate exchange, demonstrating the improved assembly and perfect orientation.

Although exchanging the long-chain ligands with thiocyanate improves the assembly in the large area monolayer case, one concern with such postsynthetic ligand exchange is always the accompanying changes in material properties.[39−41] The absorption and photoluminescence (PL) spectra of $CsPbBr_3$ are identical before and after treatment (Figure S6). However, a significant increase in the PL quantum yield (PLQY) from 72.9 to 90.9% is observed after thiocyanate treatment, which is consistent with the literature.[38] Details of the PLQY measurement are explained in the Experimental Section, and full schematic of the setup is explained in the "PLQY Measurement" section in the Supporting Information (Figure S7 and Table S1). Thiocyanate is not completely soluble in toluene but partially interacts with the surface of the cubes forming Cs/Pb−SCN bonds,[38] which is confirmed by Fourier transform infrared (FTIR) spectroscopy, as shown in Figure 3.

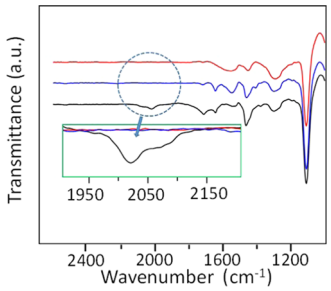

Figure 3. FTIR spectra of bare silicon (red) without thiocyanate treatment (blue) and thiocyanate-treated $CsPbBr_3$ nanocubes (black).

The inset of Figure 3 shows a broad peak around 2060 cm^{-1} that represents C≡N vibrational mode of SCN. This clearly indicates that thiocyanate binds at the surface of nanocubes and replaces some of the long hydrocarbon chains from the surface of the cubes, which is essentially the key factor for the controlled self-assembly.

We perform molecular dynamics simulations using the HOOMD-Blue software[42] with the OPLS united force field[43] and some adapted CHARMM parameters[44] to describe $CsPbBr_3$ nanocubes with either oleyls or thiocyanate at the surface (Figure S8).

We compute the free energy of assembly for a 4 × 4 two-dimensional square lattice with variable lattice constant (a_{nn}) and cube size ranging from 13 unit cells (N13—7.63 nm cube edge length) to 2 unit cells (N2—1.17 nm cube edge length) following previous methods (details in Table S2 and Figure S9).[45] Thiocyanate shows a slightly weaker attraction compared to oleyl chains for N13, as shown in Figure 4. The corresponding internal energy (U), entropy (S) and pressure (P), of the system are shown in Figure S10, displaying the usual energy entropy cancellation described in previous studies.[45] The same trends are also observed for N11, N9, N7, and N2, as shown in Figures S11−S14, respectively. In equilibrium, the system is dry (free of any toluene), and the minimum bonding free energy results from a competition between the attractive enthalpic vdW attraction and the repulsive entropic chain packing (see Figures 4 and S10). The bonding free energy is 40% stronger with oleyl chains than with thiocyanate (−1514 k_BT vs −920 k_BT for 7.63 nm cube). In both cases, the strong attractive forces are holding the cubes together. This points to a finer assembly control as the thiocyanate nanocubes only get pulled together strongly when they are already close to the proper orientation for ideal packing, whereas the former starts to have strong long-range attractive interactions for less ideal binding configurations; the longer the ligands, the more difficult it is to equilibrate the system. This is related to the strength of the vdW forces that increase very significantly with larger chains, leading to a "cascade effect" where longer ligands may wrap around the nanocrystals. This suggests that the shorter chains facilitate better monolayer assembly. Analysis of the structure of the capping ligands reveals that oleyl chains are completely stretched along the cube faces and curve along the corners (see Figure S15). A detailed formula for the equilibrium lattice constant, derived by adapting the Orbifold Topological Model[46−48] to the case of a cube geometry, is provided in Supporting Information and Figure S16.

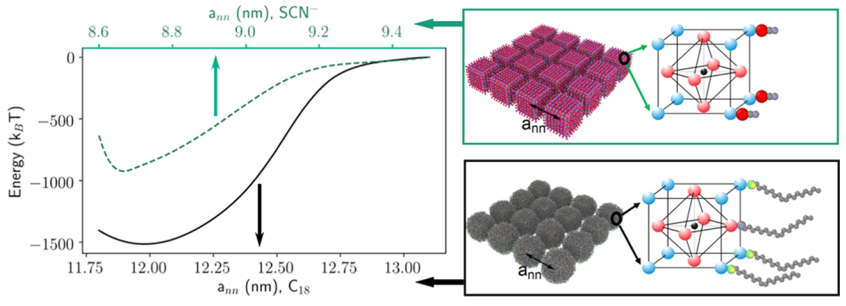

Figure 4. Free energy plots of N13 perovskite nanocubes grafted with long oleyl chains and thiocyanate. For oleyl chains, equilibrium distance (r_0) = 11.79 nm, minimum bonding free energy (F_0) = −1514 k_BT, while for thiocyanate r_0 = 8.66 nm and F_0 = −920 k_BT.

https://dx.doi.org/10.1021/acsami.0c05945
ACS Appl. Mater. Interfaces 2020, 12, 31764−31769

CONCLUSIONS

By modifying the surface of $CsPbBr_3$ perovskite nanocubes, we have described a novel route to control the interactions for self-assembly, where the long-chain hydrocarbon ligands are replaced by a shorter thiocyanate moiety. This enables high-quality nanocube self-assembly into close-packed monolayers. The monolayer films could also act as seed layers to create halide perovskite single-crystalline thin films for better performances in optoelectronic devices.

EXPERIMENTAL SECTION

Materials. Cs_2CO_3 (99.9%), lead bromide ($PbBr_2$, 99.9%), octadecene (ODE, 90%), oleylamine (OAm, 90%), oleic acid (OA, 90%), and ammonium thiocyanate (NH_4SCN, 90%) are purchased from Sigma-Aldrich. All of the chemicals are used without further purifications.

Methods. *Preparation of Cesium Oleate.* Typically, 0.814 g of Cs_2CO_3 is loaded into 100 mL three-neck flask along with 40 mL of octadecene and 2.5 mL of OA, dried for 1 h at 120 °C, and then heated under N_2 to 150 °C until all Cs_2CO_3 reacts with OA. Preheating of cesium oleate to 100 °C before injection is necessary as it precipitates out from ODE at room temperature.

Synthesis of $CsPbBr_3$ Nanocubes. In a typical synthesis, 0.188 mmol of $PbBr_2$ with 5 mL of ODE, 0.5 mL of OAm, and 0.5 mL of OA is loaded into a three-neck round bottom flask and dried under vacuum at 120 °C for an hour. Then, the reaction atmosphere is made inert by passing N_2. After complete solubilization of $PbBr_2$, the temperature is raised to 200 °C and 0.4 mL of the preheated cesium oleate is injected into the three-neck flask. After the injection, the color of the solution turns from colorless to greenish yellow, indicating the formation of perovskite cubes. Then, we lower the temperature to 160 °C and anneal the solution at that temperature for 10 min to get uniform size dispersion of the cubes. After that, we cool the solution using ice water bath for further use.

Isolation and Purification of $CsPbBr_3$ Cubes. After the synthesis, we use two-step centrifugations to collect the cubes for our self-assembly study. First, we take 1 mL from the stock solution just after the synthesis and centrifuge at 8000 rpm for 20 min to collect all $CsPbBr_3$ particles from the solution. We discard the supernatant, wash gently the inner wall of the tube using a tissue paper, and add 2 mL of toluene to disperse the whole $CsPbBr_3$ solid. Then, we perform the second step of centrifugation at 2000 rpm for 5 min to get rid of all the large particles. Now, from the supernatant, we have 2 mL of toluene containing $CsPbBr_3$ nanocubes with a size distribution around 10−15 nm.

Surface Modification of $CsPbBr_3$ Nanocubes. To get well-controlled self-assembly, we have performed surface modification of the cubes from long hydrocarbon oleyl chain to short thiocyanate ion. We use NH_4SCN as a source of thiocyanate. About 50 mg of the NH_4SCN powder is added in excess into 2 mL perovskite cube solution in toluene in a 4 mL vial containing a magnetic bar. The solution is stirred for 30 min inside a glovebox. To get rid of the insoluble NH_4SCN, we centrifuge the solution at 2000 rpm for 2 min and use the supernatant for self-assembly study. NH_4SCN is insoluble in toluene but replaces some of the oleate ligands from the surfaces of the cubes, as confirmed from FTIR spectroscopy (Figure 4).

PL Quantum Yield Measurement. We measure the PLQY using a custom-modified GPS-033-SL integrating sphere built by LabSphere.[49] A laser diode (Thorlabs, L405P20, 405 nm) is used as an excitation source, passing through an optical chopper (Thorlabs, MC2000B-EC), hitting into the integrating sphere. The incident intensity is controlled with neutral density filters (Thorlabs). The beam hits the sample within a cylindrical cuvette. Light leaving the exit port of the sphere, fitted with a baffle to prevent direct reflections, hits onto a low-noise Newport 818-SL calibrated photodetector, which is connected to a Stanford Research Systems SR830 lock-in amplifier. We measure the excitation and emission separately using a short-pass filter (Thorlabs FESH0450) and long-pass filter (Thorlabs FELH0450) in front of the photodetector. The comparison of the emission and excitation results in the quantum yield. The sensitivity as a function of wavelength is calibrated with the spectral responsivity of the photodetector. A more detailed description of this calculation can be found in the Supporting Information.

Self-Assembly Process and Theoretical Calculations. Details of the monolayer assembly including details of the setup used are described in the Supporting Information. Theoretical calculations with modeling of nanocubes to calculate the bonding free energy during the self-assembly process is also explained in Supporting Information.

Instrumentations. *UV−Vis Spectroscopy.* Absorption of $CsPbBr_3$ nanocubes in toluene is measured using a Perkin Elmer UV/VIS/NIR spectrometer.

PL Measurement. A 405 nm laser diode (Thorlabs S1FC405) is used as an excitation source, where the PL intensity of the $CsPbBr_3$ perovskites is collected in reflection mode through a NA 0.9 objective using a spectrometer (UHTC 300 VIS, WITec).

XRD. We use Bruker Cu Kα XRD to get the crystallographic orientation of our sample.

FTIR. We perform FTIR to get the surface composition of the nanocubes using VERTEX 80V Bruker instrument.

AFM. We use Veeco Dimension 3100 AFM to measure different thicknesses and to measure RMS roughness of the nanocube film.

SEM. We use the FEI Verios 460 to take all of the scanning electron microscope images shown in the manuscript.

ASSOCIATED CONTENT

Supporting Information

The Supporting Information is available free of charge at https://pubs.acs.org/doi/10.1021/acsami.0c05945.

Description of the experimental setup and some extra characterizations for monolayer assembly, PLQY measurement, and details of the theoretical calculations (PDF)

AUTHOR INFORMATION

Corresponding Author

Erik C. Garnett − *Center for Nanophotonics, AMOLF, 1098XG Amsterdam, The Netherlands;* orcid.org/0000-0002-9158-8326; Email: e.garnett@amolf.nl

Authors

Biplab K. Patra − *Center for Nanophotonics, AMOLF, 1098XG Amsterdam, The Netherlands; Materials Chemistry Department, CSIR—Institute of Minerals and Materials Technology, Bhubaneswar 751013, India;* orcid.org/0000-0003-0592-4344

Harshal Agrawal − *Center for Nanophotonics, AMOLF, 1098XG Amsterdam, The Netherlands;* orcid.org/0000-0002-5106-3947

Jian-Yao Zheng − *Center for Nanophotonics, AMOLF, 1098XG Amsterdam, The Netherlands*

Xun Zha − *Department of Physics and Astronomy, Iowa State University, Ames, Iowa 50011, United States;* orcid.org/0000-0001-9539-6172

Alex Travesset − *Department of Physics and Astronomy and Ames Laboratory, Iowa State University, Ames, Iowa 50011, United States;* orcid.org/0000-0001-7030-9570

Complete contact information is available at: https://pubs.acs.org/10.1021/acsami.0c05945

Author Contributions

⊥B.K.P. and H.A. contributed equally to this work.

https://dx.doi.org/10.1021/acsami.0c05945
ACS Appl. Mater. Interfaces 2020, 12, 31764−31769

Notes

The authors declare no competing financial interest.

■ ACKNOWLEDGMENTS

The work at AMOLF is part of the research program of the "Nederlandse Organisatie voor Wetenschappelijk Onderzoek" (NWO). This work is supported by the NWO VIDI grant (Project Number 14846). Theoretical work done for this paper uses the Extreme Science and Engineering Discovery Environment (XSEDE), which is supported by the National Science Foundation (Grant Number ACI-1548562). The project within XSEDE is supported by grant TG-MCB140071. This work is supported by NSF, DMR-CMMT 1606336 CDS&E: "Design Principles for Ordering Nanoparticles into Supercrystals".

■ REFERENCES

(1) Zhang, S. Y.; Regulacio, M. D.; Han, M. Y. Self-Assembly of Colloidal One-Dimensional Nanocrystals. *Chem. Soc. Rev.* **2014**, *43*, 2301−2323.
(2) Miszta, K.; de Graaf, J.; Bertoni, G.; Dorfs, D.; Brescia, R.; Marras, S.; Ceseracciu, L.; Cingolani, R.; van Roij, R.; Dijkstra, M.; et al. Hierarchical Self-Assembly of Suspended Branched Colloidal Nanocrystals into Superlattice Structures. *Nat. Mater.* **2011**, *10*, 872−876.
(3) Vogel, N.; Retsch, M.; Fustin, C. A.; Del Campo, A.; Jonas, U. Advances in Colloidal Assembly: The Design of Structure and Hierarchy in Two and Three Dimensions. *Chem. Rev.* **2015**, *115*, 6265−6311.
(4) Rainò, G.; Becker, M. A.; Bodnarchuk, M. I.; Mahrt, R. F.; Kovalenko, M. V.; Stöferle, T. Superfluorescence from Lead Halide Perovskite Quantum Dot Superlattices. *Nature* **2018**, *563*, 671−675.
(5) Ravi, V. K.; Scheidt, R. A.; Dubose, J.; Kamat, P. V. Hierarchical Arrays of Cesium Lead Halide Perovskite Nanocrystals through Electrophoretic Deposition. *J. Am. Chem. Soc.* **2018**, *140*, 8887−8894.
(6) Grzelczak, M.; Vermant, J.; Furst, E. M.; Liz-Marzán, L. M. Directed Self-Assembly of Nanoparticles. *ACS Nano* **2010**, *4*, 3591−3605.
(7) Singh, A.; Coughlan, C.; Laffir, F.; Ryan, K. M. Assembly of $CuIn_{1-x}Ga_xS_2$ Nanorods into Highly Ordered 2D and 3D Superstructures. *ACS Nano* **2012**, *6*, 6977−6983.
(8) Goerlitzer, E. S. A.; Taylor, R. N. K.; Vogel, N. Bioinspired Photonic Pigments from Colloidal Self-Assembly. *Adv. Mater.* **2018**, *30*, No. 1706654.
(9) Noorduin, W. L.; Grinthal, A.; Mahadevan, L.; Aizenberg, J. Rationally Designed Complex, Hierarchical Microarchitectures. *Science* **2013**, *340*, 832−837.
(10) Dong, A.; et al. Electronically Coupled Nanocrystal Superlattice Films by in Situ Ligand Exchange at the Liquid/Air Interface. *ACS Nano* **2013**, *7*, 10978−10984.
(11) Geuchies, J. J.; van Overbeek, C.; Evers, W. H.; Goris, B.; de Backer, A.; Gantapara, A. P.; Rabouw, F. T.; Hilhorst, J.; Peters, J. L.; Konovalov, O.; et al. In Situ Study of the Formation Mechanism of Two-Dimensional Superlattices from PbSe Nanocrystals. *Nat. Mater.* **2016**, *15*, 1248−1254.
(12) Pietra, F.; Rabouw, F. T.; Evers, W. H.; Byelov, D. V.; Petukhov, A. V.; De Mello Donegá, C.; Vanmaekelbergh, D. Semiconductor Nanorod Self-Assembly at the Liquid/Air Interface Studied by in Situ GISAXS and Ex Situ TEM. *Nano Lett.* **2012**, *12*, 5515−5523.
(13) Ni, S.; Isa, L.; Wolf, H. Capillary Assembly as a Tool for the Heterogeneous Integration of Micro- and Nanoscale Objects. *Soft Matter* **2018**, *14*, 2978−2995.
(14) Zhang, H.; Cadusch, J.; Kinnear, C.; James, T.; Roberts, A.; Mulvaney, P. Direct Assembly of Large Area Nanoparticle Arrays. *ACS Nano* **2018**, *12*, 7529−7537.
(15) Kister, T.; Monego, D.; Mulvaney, P.; Widmer-Cooper, A.; Kraus, T. Colloidal Stability of Apolar Nanoparticles: The Role of Particle Size and Ligand Shell Structure. *ACS Nano* **2018**, *12*, 5969−5977.
(16) Wei, W.; Wang, Y.; Ji, J.; Zuo, S.; Li, W.; Bai, F.; Fan, H. Fabrication of Large-Area Arrays of Vertically Aligned Gold Nanorods. *Nano Lett.* **2018**, *18*, 4467−4472.
(17) Baranov, D.; Toso, S.; Imran, M.; Manna, L. Investigation into the Photoluminescence Red Shift in Cesium Lead Bromide Nanocrystal Superlattices. *J. Phys. Chem. Lett.* **2019**, *10*, 655−660.
(18) Van Der Burgt, J. S.; Geuchies, J. J.; Van Der Meer, B.; Vanrompay, H.; Zanaga, D.; Zhang, Y.; Albrecht, W.; Petukhov, A. V.; Filion, L.; Bals, S.; et al. Cuboidal Supraparticles Self-Assembled from Cubic $CsPbBr_3$ Perovskite Nanocrystals. *J. Phys. Chem. C* **2018**, *122*, 15706−15712.
(19) Mehetor, S. K.; Ghosh, H.; Pradhan, N. Blue-Emitting $CsPbBr_3$ Perovskite Quantum Rods and Their Wide-Area 2D Self-Assembly. *ACS Energy Lett.* **2019**, *4*, 1437−1442.
(20) Xin, B.; Pak, Y.; Mitra, S.; Almalawi, D.; Alwadai, N.; Zhang, Y.; Roqan, I. S. Self-Patterned $CsPbBr_3$ Nanocrystals for High-Performance Optoelectronics. *ACS Appl. Mater. Interfaces* **2019**, *11*, 5223−5231.
(21) Wang, L.; Liu, B.; Zhao, X.; Demir, H. V.; Gu, H.; Sun, H. Solvent-Assisted Surface Engineering for High-Performance All-Inorganic Perovskite Nanocrystal Light-Emitting Diodes. *ACS Appl. Mater. Interfaces* **2018**, *10*, 19828−19835.
(22) Maurer, J. H. M.; González-García, L.; Reiser, B.; Kanelidis, I.; Kraus, T. Templated Self-Assembly of Ultrathin Gold Nanowires by Nanoimprinting for Transparent Flexible Electronics. *Nano Lett.* **2016**, *16*, 2921−2925.
(23) Zha, X.; Travesset, A. Stability and Free Energy of Nanocrystal Chains and Superlattices. *J. Phys. Chem. C* **2018**, *122*, 23153−23164.
(24) Waltmann, C.; Horst, N.; Travesset, A. Capping Ligand Vortices as "Atomic Orbitals" in Nanocrystal Self-Assembly. *ACS Nano* **2017**, *11*, 11273−11282.
(25) He, X.; Qiu, Y.; Yang, S. Fully-Inorganic Trihalide Perovskite Nanocrystals: A New Research Frontier of Optoelectronic Materials. *Adv. Mater.* **2017**, *29*, No. 1700775.
(26) Akkerman, Q. A.; Rainò, G.; Kovalenko, M. V.; Manna, L. Genesis, Challenges and Opportunities for Colloidal Lead Halide Perovskite Nanocrystals. *Nat. Mater.* **2018**, *17*, 394−405.
(27) Shamsi, J.; Urban, A. S.; Imran, M.; De Trizio, L.; Manna, L. Metal Halide Perovskite Nanocrystals: Synthesis, Post-Synthesis Modifications, and Their Optical Properties. *Chem. Rev.* **2019**, *119*, 3296−3348.
(28) Protesescu, L.; Yakunin, S.; Bodnarchuk, M. I.; Krieg, F.; Caputo, R.; Hendon, C. H.; Yang, R. X.; Walsh, A.; Kovalenko, M. V. Nanocrystals of Cesium Lead Halide Perovskites ($CsPbX_3$, X = Cl, Br, and I): Novel Optoelectronic Materials Showing Bright Emission with Wide Color Gamut. *Nano Lett.* **2015**, *15*, 3692−3696.
(29) Zhang, D.; Yu, Y.; Bekenstein, Y.; Wong, A. B.; Alivisatos, A. P.; Yang, P. Ultrathin Colloidal Cesium Lead Halide Perovskite Nanowires. *J. Am. Chem. Soc.* **2016**, *138*, 13155−13158.
(30) Dou, L.; Lai, M.; Kley, C. S.; Yang, Y.; Bischak, C. G.; Zhang, D.; Eaton, S. W.; Ginsberg, N. S.; Yang, P. Spatially Resolved Multicolor $CsPbX_3$ Nanowire Heterojunctions via Anion Exchange. *Proc. Natl. Acad. Sci. U.S.A.* **2017**, *114*, 7216−7221.
(31) Shamsi, J.; Dang, Z.; Bianchini, P.; Canale, C.; Di Stasio, F.; Brescia, R.; Prato, M.; Manna, L. Colloidal Synthesis of Quantum Confined Single Crystal $CsPbBr_3$ Nanosheets with Lateral Size Control up to the Micrometer Range. *J. Am. Chem. Soc.* **2016**, *138*, 7240−7243.
(32) Polavarapu, L.; Tong, Y.; Bohn, B. J.; Bladt, E.; Wang, K.; Müller-Buschbaum, P.; Bals, S.; Urban, A. S.; Feldmann, J. Precursor Powders-to-$CsPbX_3$ Perovksite Nanowires: One-Pot Synthesis, Growth Mechanism and Oriented Self-Assemblies. *Angew. Chem., Int. Ed.* **2017**, *129*, 13887−13892.
(33) Sun, J.-K.; Huang, S.; Liu, X.-Z.; Xu, Q.; Zhang, Q.-H.; Jiang, W.-J.; Xue, D.-J.; Xu, J.-C.; Ma, J.-Y.; Ding, J.; et al. Polar Solvent

https://dx.doi.org/10.1021/acsami.0c05945
ACS Appl. Mater. Interfaces 2020, 12, 31764−31769

Induced Lattice Distortion of Cubic $CsPbI_3$ Nanocubes and Hierarchical Self-Assembly into Orthorhombic Single-Crystalline Nanowires. *J. Am. Chem. Soc.* **2018**, *140*, 11705−11715.
(34) Nagaoka, Y.; Hills-Kimball, K.; Tan, R.; Li, R.; Wang, Z.; Chen, O. Nanocube Superlattices of Cesium Lead Bromide Perovskites and Pressure-Induced Phase Transformations at Atomic and Mesoscale Levels. *Adv. Mater.* **2017**, *29*, No. 1606666.
(35) Gomez, L.; Lin, J.; de Weerd, C.; Poirier, L.; Boehme, S. C.; von Hauff, E.; Fujiwara, Y.; Suenaga, K.; Gregorkiewicz, T. Extraordinary Interfacial Stitching between Single All-Inorganic Perovskite Nanocrystals. *ACS Appl. Mater. Interfaces* **2018**, *10*, 5984−5991.
(36) Hudait, B.; Dutta, S. K.; Patra, A.; Nasipuri, D.; Pradhan, N. Facets Directed Connecting Perovskite Nanocrystals. *J. Am. Chem. Soc.* **2020**, *142*, 7207−7217.
(37) Yang, Y.; Lee, J. T.; Liyanage, T.; Sardar, R. Flexible Polymer-Assisted Mesoscale Self-Assembly of Colloidal $CsPbBr_3$ Perovskite Nanocrystals into Higher Order Superstructures with Strong Inter-Nanocrystal Electronic Coupling. *J. Am. Chem. Soc.* **2019**, *141*, 1526−1536.
(38) Koscher, B. A.; Swabeck, J. K.; Bronstein, N. D.; Alivisatos, A. P. Essentially Trap-Free $CsPbBr_3$ Colloidal Nanocrystals by Postsynthetic Thiocyanate Surface Treatment. *J. Am. Chem. Soc.* **2017**, *139*, 6566−6569.
(39) Liu, Z.; Bekenstein, Y.; Ye, X.; Nguyen, S. C.; Swabeck, J.; Zhang, D.; Lee, S. T.; Yang, P.; Ma, W.; Alivisatos, A. P. Ligand Mediated Transformation of Cesium Lead Bromide Perovskite Nanocrystals to Lead Depleted Cs_4PbBr_6 Nanocrystals. *J. Am. Chem. Soc.* **2017**, *139*, 5309−5312.
(40) Balakrishnan, S. K.; Kamat, P. V. Ligand Assisted Transformation of Cubic $CsPbBr_3$ Nanocrystals into Two-Dimensional $CsPb_2Br_5$ Nanosheets. *Chem. Mater.* **2018**, *30*, 74−78.
(41) Udayabhaskararao, T.; Houben, L.; Cohen, H.; Menahem, M.; Pinkas, I.; Avram, L.; Wolf, T.; Teitelboim, A.; Leskes, M.; Yaffe, O.; et al. A Mechanistic Study of Phase Transformation in Perovskite Nanocrystals Driven by Ligand Passivation. *Chem. Mater.* **2018**, *30*, 84−93.
(42) Anderson, J. A.; Lorenz, C. D.; Travesset, A. General Purpose Molecular Dynamics Simulations Fully Implemented on Graphics Processing Units. *J. Comput. Phys.* **2008**, *227*, 5342−5359.
(43) Jorgensen, W. L.; Madura, J. D.; Swenson, C. J. Optimized Intermolecular Potential Functions for Liquid Hydrocarbons. *J. Am. Chem. Soc.* **1984**, *106*, 6638−6646.
(44) Brooks, B. R.; Brooks, C. L.; Mackerell, A. D.; Nilsson, L.; Petrella, R. J.; Roux, B.; Won, Y.; Archontis, G.; Bartels, C.; Boresch, S.; et al. CHARMM: The Biomolecular Simulation Program. *J. Comput. Chem.* **2009**, *30*, 1545−1614.
(45) Zha, X.; Travesset, A. Stability and Free Energy of Nanocrystal Chains and Superlattices. *J. Phys. Chem. C* **2018**, *122*, 23153−23164.
(46) Landman, U.; Luedtke, W. D. Small Is Different: Energetic, Structural, Thermal, and Mechanical Properties of Passivated Nanocluster Assemblies. *Faraday Discuss.* **2004**, *125*, 1−22.
(47) Travesset, A. Soft Skyrmions, Spontaneous Valence and Selection Rules in Nanoparticle Superlattices. *ACS Nano* **2017**, *11*, 5375−5382.
(48) Travesset, A. Topological Structure Prediction in Binary Nanoparticle Superlattices. *Soft Matter* **2017**, *13*, 147−157.
(49) de Mello, J. C.; Wittmann, H. F.; Friend, R. H. An Improved Experimental Determination of External Photoluminescence Quantum efficiency. *Adv. Mater.* **1997**, *9*, 230−232.

https://dx.doi.org/10.1021/acsami.0c05945
ACS Appl. Mater. Interfaces 2020, 12, 31764−31769